Progress in NUCLEAR SCIENCE and TECHNOLOGY, Vol. 2, pp.9-15 (2011)

ARTICLE

Hydrogen–Grain Boundary Interaction in Fe, Fe–C, and Fe–N Systems

Ryosuke MATSUMOTO [1,*], Marika RIKU [1], Shinya TAKETOMI [2] and Noriyuki MIYAZAKI [1]

[1]*Department of Mechanical Engineering and Science, Graduate School of Engineering, Kyoto University, Yoshida-Honmachi, Sakyo-ku, 606-8501 Kyoto, Japan*
[2]*Department of Mechanical Engineering, Graduate School of Science and Engineering, Saga University, 1 Honjo-machi, Saga-city, 840-8502 Saga, Japan*

Highly accurate predictions of hydrogen's influence on material strength and development of materials with minimal hydrogen effects are essential to prevent failure under various hydrogen environments. Here, we investigated the influence of misorientation angle and solute elements (carbon and nitrogen) on the cohesive energy of <110> symmetrical tilt grain boundaries (STGBs) in bcc Fe under a gaseous hydrogen environment by using density functional theory. We found a good correlation among GB energy, GB free volume, and the hydrogen concentration at GBs under hydrogen environments: high-energy GBs have large gaps, and many hydrogen atoms are captured at these spaces. Thus, higher-energy GBs are more influenced by hydrogen. It is also shown that the binding energy between hydrogen and a GB is negligible when nitrogen or carbon atoms exist at the GB at their solubility limit. Therefore, carbon and nitrogen atoms exclude hydrogen atoms from GBs and improve the cohesive energy of GBs under hydrogen environments.

KEYWORDS: density functional theory, grain boundary, cohesive energy, hydrogen, carbon, nitrogen, embrittlement, binding energy, concentration

I. Introduction

Highly accurate predictions of hydrogen's influence on material strength and development of materials with minimal hydrogen effects are essential to prevent failure under various hydrogen environments. Therefore, it is important to know the fundamental effect of each grain boundary (GB) property, such as stability and chemical composition, on the hydrogen sensitivity of material strength, because it has been reported that higher-strength steels tend to experience intergranular fracture under hydrogen environments.[1-3)]

It has been experimentally reported that the strength of materials under hydrogen environments is improved by the control of the distribution of misorientation angles of GBs.[4)] Farkas et al. estimated the hydrogen effect on the cohesive energy of GBs by using the embedded-atom-method (EAM) potential developed by Ruda *et al*.[5,6)] Furthermore, Yamaguchi and Gesari evaluated the hydrogen binding energy and cohesive energy of GBs by using a density-functional-theory (DFT) calculation, and showed that hydrogen has an embrittling effect on GBs.[7,8)] However, the hydrogen concentration at GBs and the cohesive energy under a practical hydrogen environment have not yet been clarified. For example, it is still difficult to experimentally determine the hydrogen concentration at individual GBs. Some theoretical calculations of the cohesive energy of GBs have used extremely high hydrogen concentrations.

Here, by using DFT calculations, we estimated the influence of the misorientation angle on the hydrogen concentration at GBs in bcc Fe under a practical gaseous hydrogen environment, and obtained the cohesive energy of GBs with the thermal equilibrium hydrogen concentration. We also investigated the influence of solute elements (carbon and nitrogen) on the hydrogen concentration and cohesive energy of GBs.

II. Methods

1. Density Functional Theory

We performed DFT calculations within the spin-polarized generalized gradient approximation[9)] for electron exchange and correlation by using the Vienna *ab initio* simulation package (VASP).[10-12)] The interactions between the ions and electrons are described by Blöchl's projector-augmented-wave method,[13)] whose accuracy corresponds to an all-electron method within the frozen-core approximation. The Monkhorst–Pack scheme[14)] is used to define the *k* points, and the conjugate-gradient (CG) method is employed for the relaxation algorithm.

We employed a $10 \times 10 \times 10$ *k*-point mesh for the conventional bcc unit lattice and a cut-off energy of 425 eV. Zero-point-energy corrections, calculated from the Hessian matrix, were considered for hydrogen, nitrogen, and carbon atoms. In all calculations, the supercell method (three-dimensional periodic boundary condition) was applied.

2. Preparation of GB Models

In this study, we used a <110> symmetrical tilt grain

*Corresponding author, E-mail: matsumoto@solid.me.kyoto-u.ac.jp

boundary (STGB) for the ease of treatment. The model preparation was conducted via the following process.

1) Bonding of two crystals: Two rectangular parallelepiped crystals with the intended orientation are joined. In our calculation method, the three-dimensional periodic boundary condition is applied, and thus, two GBs with the same misorientation angle are formed in the unit cell. We placed the *xy*-plane at a GB plane so that the *x*-axis is placed along the <110> axis. For the DFT calculations, we used three GB models with different misorientation angles ϕ: Σ3(111) STGB (ϕ = 70.5°), Σ3(112) STGB (ϕ = 109.5°), and Σ9(114) STGB (ϕ = 141.1°).
2) Elimination of excessively close atomic pairs: The interatomic distance between some of the atomic pairs near the interface may become excessively close after the artificial bonding of crystals in the previous procedure. Therefore, when the interatomic distance was closer than a critical distance r_c, we removed one atom of such a pair, and placed the other at the midpoint of the initial positions. We performed some preliminary calculations for different lengths of r_c, and then used $r_c = 0.8 \times a$ because it gave minimum energy for various GBs. Here, a is the nearest-neighbor distance in bcc Fe (≈0.287 nm).
3) Relaxation of the GB model: We performed relaxation of atomic configuration and simulation cell size by the CG method. The model size is 0.40 × 0.70 × 1.55 nm^3 (36 Fe atoms) for Σ3(111) STGB, 0.41 × 0.50 × 1.43 nm^3 (24 Fe atoms) for Σ3(112) STGB, and 0.40 × 0.86 × 2.35 nm^3 (68 Fe atoms) for Σ9(114) STGB. The atomic configurations and the coordinate system are shown in **Fig. 1**.

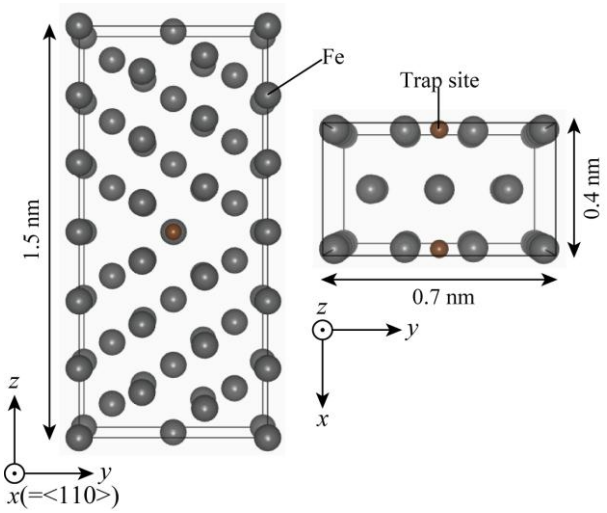

(a) Σ3(111) STGB (ϕ = 70.5°)

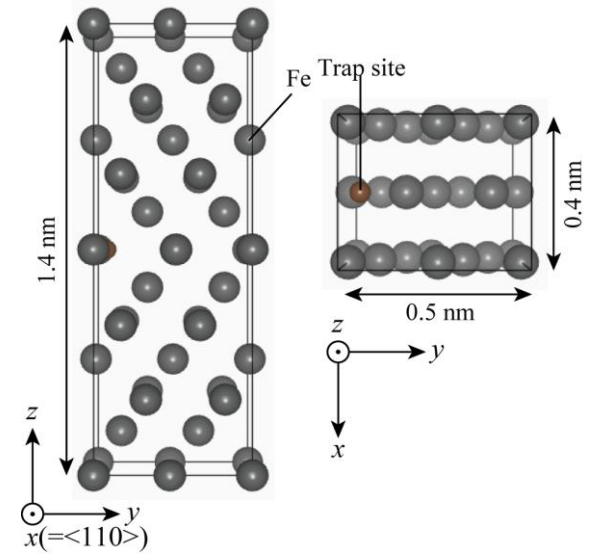

(b) Σ3(112) STGB (ϕ = 109.5°)

Fig. 1 Atomic configurations of GB models: Trap sites indicated in the figures have the strongest binding energy, as discussed in the text.

3. Evaluation of GB Properties

(1) GB Energy and GB Free Volume

A system with GBs has higher energy compared to a perfect crystal. We estimated the GB energy by the following equation:[15)]

$$E_{GB} = \frac{\Phi_{Fe\_GB} - n \times \phi_{Fe}}{2S} \quad (1)$$

Here, S is the area of a GB in the simulation cell, Φ_{Fe_GB} is the energy of the system with a GB, ϕ_{Fe} is the energy of one atom at the undeformed bcc structure, and n is the number of Fe atoms in the GB model.

To quantify the total gap around the GB, we evaluated the GB free volume as the excess volume per unit GB area by the following equation[16,17)]:

$$\Omega = \frac{V_{Fe\_GB} - n \times v_{Fe}}{2S} \quad (2)$$

Here, V_{Fe_GB} is the volume of the system with a GB and v_{Fe} is the volume of one atom at the undeformed bcc structure.

(2) Binding Energy

We estimated the binding energy between a GB and a solute atom (hydrogen, nitrogen, or carbon) by the following procedure.

1) Determination of the initial position of a solute atom: Hydrogen, nitrogen, and carbon atoms exist in bcc Fe predominantly as interstitial atoms. There are two types of occupation sites for interstitial atoms within the bcc lattice: one is the tetrahedral site (T-site) and the other is the octahedral site (O-site). The T-site is the more stable occupation site for a hydrogen atom in bcc Fe,[18)] while the O-site is the more stable occupation site for carbon and nitrogen atoms.[19,20)] However, the stable occupation site possibly changes depending on the strain.[18,21)] Here, we deal with the disordered crystalline region near the GB, and therefore, an interstitial atom within both T- and O-sites is considered. Here, T-sites within the perfect bcc lattice correspond to the vertices

of a Voronoi polyhedron, and O-sites are located at the center of a square on the polyhedron surfaces.[22] The initial occupation sites of the solute atoms were defined using these rules.

2) Relaxation of the system with a solute atom: We introduced a solute atom into an occupation site positioned at $\boldsymbol{x}$, and performed relaxation of atomic configuration and simulation cell size by using the CG method. Subsequent to the relaxation, we obtained the energy of the system $\Phi_{\mathrm{Fe\_GB+X}}$.

3) Estimation of binding energy: The heat of solution (HOS) of a solute atom in position $\boldsymbol{x}$ is calculated by the following equation:

$$E^{\mathrm{HOS}}(\boldsymbol{x}) = \Phi_{\mathrm{Fe\_GB+X}}(\boldsymbol{x}) - \left(\Phi_{\mathrm{Fe\_GB}} + \Phi_{\mathrm{X}}\right) \tag{3}$$

Here, Φ_{X} is the energy of a solute atom in vacuum. The terms cancel out in Equation (4) as described below, and thus, the exact value of Φ_{X} is unnecessary.

We defined the binding energy[a] between the GB and the solute atom positioned at $\boldsymbol{x}$ by the difference between the HOS into position $\boldsymbol{x}$ and a position far from the GB. HOS into a position far from the GB corresponds to HOS into a perfect lattice $E^{\mathrm{HOS\_Lattice}}$, and thus, the binding energy is estimated by the following equation:

$$E(\mathrm{x}) = E^{\mathrm{HOS\_Lattice}} - E^{\mathrm{HOS}}(\boldsymbol{x}) \tag{4}$$

4) Estimation of the binding energy distribution: We obtained the distribution of the binding energy around the GBs by repeating steps 2) and 3) for each occupation site evaluated in step 1).

(3) Occupancy of a Solute Atom at a Trap Site

The occupancy of a solute atom at a specific site c_i with binding energy E_i is given by the following equation under a thermal equilibrium condition:[23,24]

$$\frac{c_i}{1-c_i} = \frac{c_{\mathrm{Lattice}}}{1-c_{\mathrm{Lattice}}} \exp\left(\frac{E_i}{k_{\mathrm{B}}T}\right) \tag{5}$$

Here, k_{B} and T are the Boltzmann constant and temperature, respectively. c_{Lattice} is the occupancy of a solute atom at an occupation site within the undeformed bcc lattice (T-site for hydrogen and O-site for nitrogen and carbon). We used the following values for c_{Lattice}:

1) Hydrogen atom: Hirth has reported the hydrogen concentration (atomic fraction of hydrogen) for high-purity iron under gaseous hydrogen environments based on Sievert's law.[25] Subsequent to some unit conversion, the hydrogen occupancy at the T-site under thermal equilibrium conditions is given by the following equation as a function of hydrogen gas pressure p (Pa) and temperature T (K):

$$c_{\mathrm{Lattice}} = 0.9686 \times 10^{-6} \sqrt{p} \exp\left(-\frac{3440}{T}\right) \tag{6}$$

This relationship corresponds to the theoretical estimation performed by Sugimoto and Fukai.[26] Using Eq. (6), we obtained the hydrogen concentration under a practical gaseous hydrogen environment for storage tank and piping components.

2) Nitrogen and carbon atoms: We used the solid solubility limit into bcc Fe, i.e., 0.0075 wt.% for nitrogen (487 K) and 0.006 wt.% for carbon (room temperature).[27] Although the temperature at which solubility limit of N is obtained is not room temperature, we consider that this influence on the following discussion is very small.

Figure 2 shows the relationship between binding energy and site occupancy estimated by Eq. (5). Carbon and nitrogen atoms do not diffuse at 300 K sufficiently. The site occupancy corresponds to the condition that carbon and nitrogen atoms are assumed to be fully segregated at GB. Occupation sites with binding energy higher than ~0.25 eV are important for nitrogen and carbon atoms, and those higher than ~0.4 eV are important for hydrogen atoms under gaseous hydrogen environments.

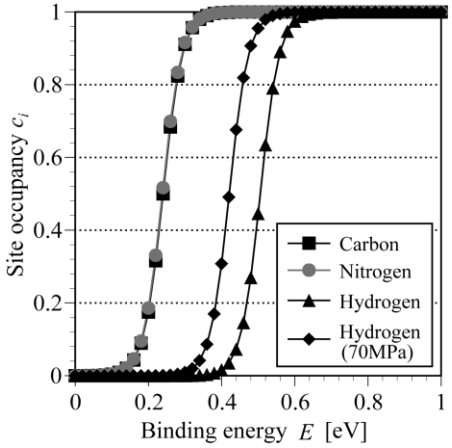

Fig. 2 Relationship between binding energy and site occupancy of carbon, nitrogen, and hydrogen. Room temperature (T = 300 K) was used for the calculations. The site occupancy was estimated under ordinary (p = 0.1 MPa ($c_{\mathrm{Lattice}} = 3.19 \times 10^{-9}$)) and high pressure ($p$ = 70 MPa ($c_{\mathrm{Lattice}} = 8.49 \times 10^{-8}$)) environments for hydrogen.

(4) Hydrogen Concentration at GB

We evaluated the hydrogen concentration at the GB as the number of hydrogen atoms per unit area of the GB; it was calculated by the summation of hydrogen occupancy at all possible sites around the GB, as shown in following equation:

$$N_{\mathrm{Total}} = \sum_i c_i n_i \tag{7}$$

[a] The value is frequently called trap energy for hydrogen atoms and segregation energy for other atoms. Here, we use binding energy for the unified treatment.

Here n_i is the number of occupation sites per unit area of GB with binding energy E_i (site density).

(5) Cohesive Energy

We evaluated the cohesive energy of the GB without a solute atom γ^0_{coh} by the following equation:

$$\gamma^0_{\mathrm{coh}} = \frac{\Phi_{\mathrm{Fe\_FS}} - \Phi_{\mathrm{Fe\_GB}}}{S} \tag{8}$$

Here, $\Phi_{\mathrm{Fe\_FS}}$ is the energy of the system with free surfaces that are formed at a GB plane.

We estimated the cohesive energy of the GB with solute atoms near the GB plane γ_{coh} as follows. Usually, most strong binding sites exist very close to a GB plane. Therefore, when the material is separated at the GB plane, several solute atoms appear on the surfaces. Thus, γ_{coh} is approximately estimated using the binding energy between the surface and the solute atoms by the following equation:[28)]

$$\gamma_{\mathrm{coh}} = \gamma^0_{\mathrm{coh}} - \sum_i c_i \left(E^{\mathrm{FS}} - E_i^{\mathrm{Trap}} \right) n_i \tag{9}$$

We evaluated E^{FS} of {111} surface using DFT calculations, and obtained E^{FS} = 0.85 eV for hydrogen, 1.09 eV for nitrogen, and 0.41 eV for carbon atoms.

III. Results and Discussion

1. Hydrogen Concentration at GBs in bcc Fe

The hydrogen binding energy and site density around the three GBs are shown in **Table 1**. Figure 2 and Table 1 indicate that the hydrogen occupancy is high only for the first and second strongest sites in Σ3(111) and strongest site in Σ9(114). **Figure 3** shows the relationship between misorientation angle and hydrogen concentration at GBs calculated by Eq. (7). Here, we assumed a high-pressure gaseous hydrogen environment and used 300 K and 70 MPa for the calculation of c_{Lattice}. **Figure 4** shows the dependences of GB energy and GB free volume on the misorientation angle. Figures 3 and 4 also indicate the values calculated using EAM potential developed by Wen *et al*. (EAM-W).[29,30)] These figures clearly show that there is a suitable correlation among GB energy, GB free volume, and the number of hydrogen atoms: high-energy GBs have large gaps, and many hydrogen atoms are trapped in these spaces. We consider that this conclusion can be applied for the GBs with the same misorientation angle and different GB energy. The results from the EAM-W potential and the DFT calculations qualitatively agree well, and thus, although the DFT calculations were performed for only three GBs because of calculation cost limitation, the relationships are justified for various GBs.

Table 1 Hydrogen binding energy and site density in <110> axis STGBs: Site 1 and Site 2 indicate the first and second strongest binding energy, respectively. Site 1 corresponds to the trap site in Fig. 1.

	Binding energy [eV] (Site density [atom/nm^2])	
	Site 1	Site 2
Σ3(111) STGB	0.49 (7.3)	0.49 (14.6)
Σ3(112) STGB	0.34 (10.3)	0.084 (20.5)
Σ9(114) STGB	0.47 (5.9)	0.37 (11.8)

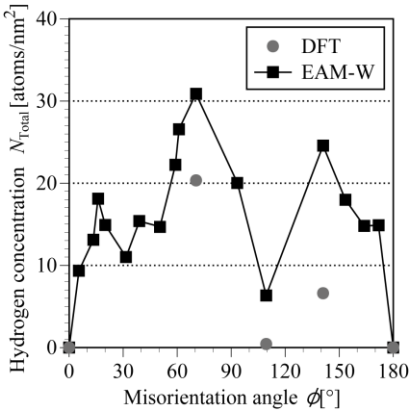

Fig. 3 Hydrogen concentration at <110> axis STGB under gaseous hydrogen environment (300 K, 70 MPa)

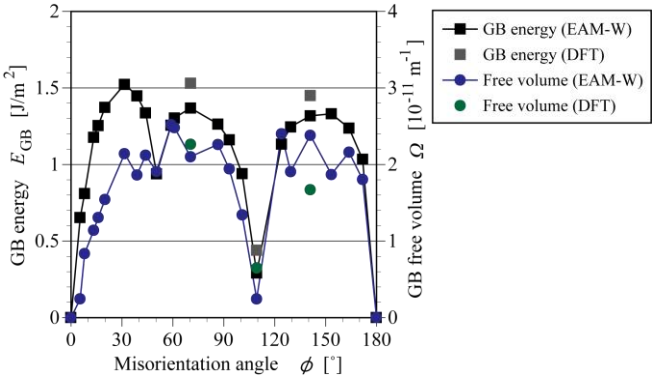

Fig. 4 Dependence of GB energy and GB free volume on the misorientation angle of <110> axis STGB

2. Cohesive Energy of GB in bcc Fe under the Gaseous Hydrogen Environment

Figure 5 shows the cohesive energy of the GBs calculated by Eq. (9). Here, we show the results for the high-pressure gaseous hydrogen condition (T = 300 K and p = 70 MPa) and the without hydrogen condition. The figure also shows the results obtained by EAM-W potential. Figure 5 confirms that hydrogen weakens the cohesive energy of GBs in bcc Fe. The discrepancy between the results obtained from the EAM-W potential and those obtained from the DFT calculation is mainly attributed to the error of surface energies obtained from the EAM-W potential. However, for both the results, comparing Figs. 4 and 5, it is found that GBs with higher GB energy, such as Σ3(111) STGB (ϕ = 70.5°) and Σ9(114) STGB (ϕ = 141.1°), have lower cohesive energy, and the influence of hydrogen is stronger for those GBs. From the DFT calculations, the reduction of cohesive energy was estimated to be about 25% for Σ3(111) STGB (ϕ = 70.5°) and almost zero for Σ3(112) STGB (ϕ = 109.5°).

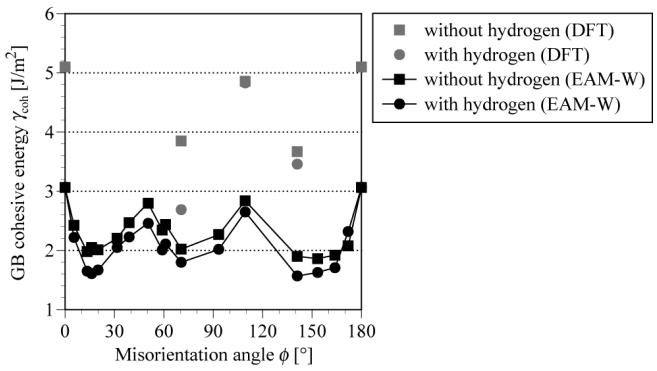

Fig. 5 Cohesive energy of <110> axis STGB with and without hydrogen atoms: For the calculation of "with hydrogen" condition, we used T = 300 K and p = 70 MPa.

3. Hydrogen Concentration at GB with Carbon or Nitrogen Atoms

Here, we used Σ3(111) STGB, which is the GB most affected by hydrogen. From our preliminarily calculations, it is confirmed that nitrogen and carbon atoms have much stronger binding energy with the GB than the hydrogen atom. Thus, under the thermal equilibrium condition, these atoms are in occupation sites. First, we find the occupation site of carbon and nitrogen around the GB, and the concentration of those atoms.

We introduced multiple carbon or nitrogen atoms into the occupation sites indicated by a–f in **Fig. 6**(a) in their order of stability[b], and estimated the binding energy for the *i*th atom (**Fig. 7**). Comparing Figs. 2 and 7, it is revealed that the occupancy of the first and second atoms is almost one; on the other hand, the occupancy is very small for the third and higher atoms for both the elements. Henceforth, we treat Σ3(111) STGB with two nitrogen or carbon atoms at the stable occupation sites, which is indicated in **Fig. 6**(b) by X. These sites are also the strongest for the hydrogen atom, and thus, hydrogen atoms are excluded from these occupation sites. We introduced a hydrogen atom at a site indicated in Fig. 6(b) by c–f and estimated the binding energy; the result is shown in **Table 2**. From these calculation results, it is found that the binding energy between hydrogen and the GB is negligible in the presence of nitrogen or carbon atoms at the GB at their solubility limit. From Fig. 2, it is clear that the hydrogen occupancy is negligible for very high-pressure gaseous environments.

Table 2 Hydrogen binding energies in Σ3(111) STGB with carbon and nitrogen atoms

Hydrogen occupation site	Hydrogen binding energy [eV] with 2 carbon atoms [atom/cell]	with 2 nitrogen atoms [atom/cell]
c, d, e, f	0.0038	−0.037

[b] The binding energy was very small for the other sites defined by Voronoi tessellation.

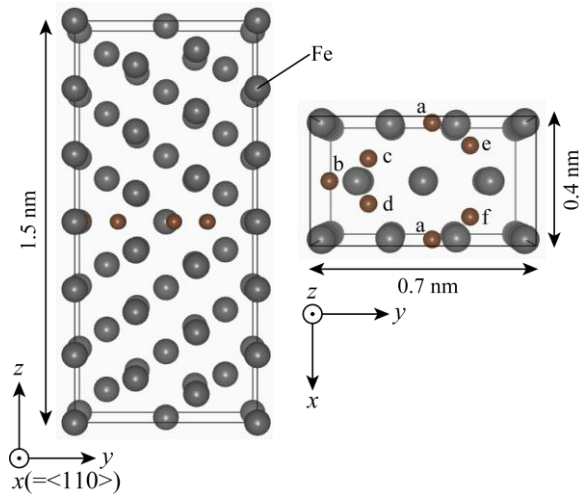

(a) Insertion sites of carbon and nitrogen atoms: multiple nitrogen or carbon atoms are introduced into a–f sites.

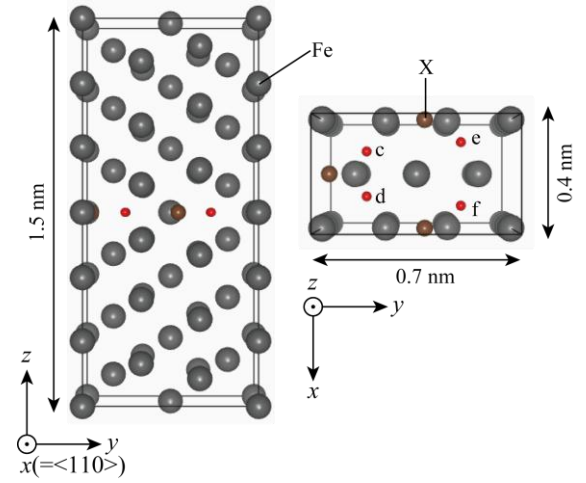

(b) Insertion sites of hydrogen atoms: two carbon atoms or two nitrogen atoms are introduced into position X, and a hydrogen atom is introduced into c–f sites.

Fig. 6 Analysis model for the estimation of the carbon and nitrogen atoms' influence on hydrogen–GB interaction (Σ3(111) STGB)

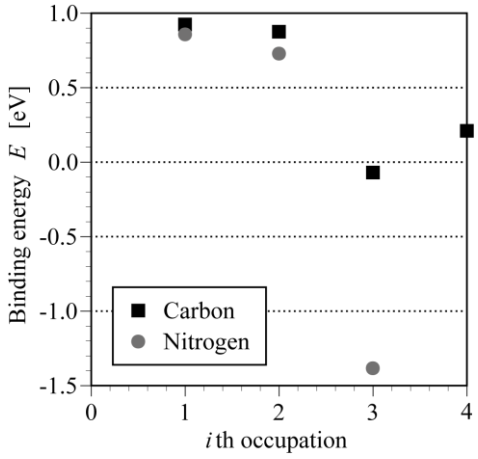

Fig. 7 Binding energy for the *i*th occupation of carbon or nitrogen atom

4. Influence of Carbon and Nitrogen on the Cohesive Energy

As shown in the previous section, hydrogen occupancy around the GB is negligible in the presence of nitrogen or carbon atoms. Thus, we estimate here the cohesive energy of the GB with only carbon or nitrogen atoms for its value under a hydrogen gaseous environment. **Table 3** shows the influence of each element on the cohesive energy at ordinary temperature and pressures (T = 300 K, p = 0.1 MPa). The table also shows the cohesive energy of a pure Fe system. The result showed that carbon atoms strengthen the GB, while nitrogen weakens it. There are various reports on the influence of nitrogen on the GB's cohesive energy in bcc Fe.[31,32] The result supports the embrittling effect. From our results, although nitrogen atoms reduce the GB's cohesive energy, the reduction rate is smaller than that by hydrogen, and thus, nitrogen, which prevent hydrogen atoms to occupy the GB, also improves the strength of the GB under hydrogen environments.

Table 3 Influence of carbon or nitrogen atoms on the cohesive energy of Σ3(111) STGB under hydrogen gaseous environment (T = 300 K, p = 0.1 MPa).

Solute elements	Cohesive energy of GB [J/m^2]	Rate of change [%]
-	3.85	-
Hydrogen	3.41	−11.3
Carbon	4.45	15.6
Nitrogen	3.58	−7.0

IV. Conclusion

In this paper, using DFT calculations, we estimated the hydrogen concentration around the <110> axis STGB in bcc Fe under hydrogen gaseous environments, and obtained the cohesive energy of the GBs. We also determined the influence of carbon and nitrogen atoms on them. The following conclusions were obtained.

1) There is a good correlation among GB energy, GB free volume, and hydrogen concentration at GB under hydrogen environments: high-energy GBs have large gaps, and many hydrogen atoms are captured at these spaces. Thus, GBs with higher GB energy are more influenced by hydrogen. The reduction in the cohesive energy was estimated to be about 25% for the high-energy GB under the high-pressure hydrogen environment (T = 300 K and p = 70 MPa).
2) The binding energy between hydrogen and the GB is negligible under the assumption that carbon and nitrogen atoms are fully segregated at GB at their solubility limit. Therefore, carbon and nitrogen atoms exclude hydrogen atoms from the GBs, and improve the cohesive energy of the GBs under hydrogen environments.

References

1) S. Matsuyama, "Delayed fracture of high strength steels," *Tetsu-to-Hagane*, **80**[9], 679-684 (1994), [in Japanese].
2) S. Hinotani, F. Terasaki, K. Takahashi, "Hydrogen embrittlement of high strength steel in high pressure hydrogen gas at ambient temperature," *Zairyo-to-Kankyo*, **64**[7], 899-905 (1978), [in Japanese].
3) X.-Y. Liu, J. Kameda, J. W. Anderegg, S. Takaki, K. Abiko, C. J. McMahon, "Hydrogen-induced cracking in a very-high-purity high-strength steel," *Mater. Sci. Eng.*, **A492**[1-2], 218-220 (2008).
4) S. Bechtle, M. Kumar, B. P. Somerday, M. E. Launey, R. O. Ritchie, "Grain-boundary engineering markedly reduces susceptibility to intergranular hydrogen embrittlement in metallic materials," *Acta Mater.*, **57**[14], 4148-4157 (2009).
5) D. Farkas, R. Nogueira, M. Ruda, B. Hyde, "Atomistic simulations of the effects of segregated elements on grain-boundary fracture in body-centered-cubic Fe," *Metall. Mater. Trans.*, **A36**[8], 2067-2072 (2005).
6) M. Ruda, D. Farkas, J. Abriata, "Embedded-atom interatomic potentials for hydrogen in metals and intermetallic alloys," *Phys. Rev.*, **B54**[14], 9765-9774 (1996).
7) M. Yamaguchi, "First-principles calculations of the grain-boundary cohesive energy -embrittling or strengthening effect of solute segregation in a bcc FeΣ3(111) grain boundary-," *J. Japan Inst. Metals*, **72**[9], 657-666 (2008), [in Japanese].
8) S. Gesari, B. Irigoyen, A. Juan, "Segregation of H, C and B to Σ=5 (013) α-Fe grain boundary: a theoretical study," *Appl. Surf. Sci.*, **253**[4], 1939-1945 (2006).
9) J. P. Perdew, Y. Wang, "Accurate and simple analytic representation of the electron-gas correlation energy," *Phys. Rev.*, **B45**[23], 13244-13249 (1992).
10) G. Kresse, J. Hafner, "Abinitio molecular-dynamics for open-shell transition-metals," *Phys. Rev.*, **B48**[17], 13115-13118 (1993).
11) G. Kresse, J. Furthmüller, "Efficient iterative schemes for ab initio total-energy calculations using a plane-wave basis set," *Phys. Rev.*, **B54**[16], 11169-11186 (1996).
12) G. Kresse, J. Furthmüller, "Efficiency of ab-initio total energy calculations for metals and semiconductors using a plane-wave basis set," *Comp. Mater. Sci.*, **6**[1], 15-50 (1996).
13) P. E. Blöchl, "Projector augmented-wave method," *Phys. Rev.*, **B50**[24], 17953-17979 (1994).
14) H. J. Monkhorst, J. D. Pack, "Special points for Brillouin-zone integrations," *Phys. Rev.*, **B13**[12], 5188-5192 (1976).
15) D. Wolf, "Correlation between the energy and structure of grain boundaries in b.c.c. metals II. symmetrical tilt boundaries," *Philo. Mag.*, **A64**[4], 447-464 (1990).
16) D. Wolf, "Correlation between energy and volume expansion for grain boundaries in fcc metals," *Scr. Metall.*, **23**[11], 1913-1918 (1989).
17) D. Wolf, "Structure-energy correlation for grain boundaries in f.c.c. metals-I. boundaries on the (111) and (100) planes," *Acta Metall.*, **37**[7], 1983-1993 (1989).
18) R. Matsumoto, Y. Inoue, S. Taketomi, N. Miyazaki, "Influence of shear strain on the hydrogen trapped in bcc-Fe: a first-principles-based study," *Scr. Mater.*, **60**[7], 555-558 (2009).
19) C. S. Becquart, C. Domain, J. Foct, "Ab initio calculations of some atomic and point defect interactions involving C and N in Fe," *Philo. Mag.*, **85**[4-7], 533-540 (2005).

20) C. Domain, C. S. Becquart, J. Foct, "Ab initio study of foreign interstitial atom (C, N) interactions with intrinsic point defects in α-Fe," P*hys. Rev.*, **B69**[14], 144112 (2004).
21) A. W. Cochardt, G. Schoek, H. Wiedersich, "Interaction between dislocations and interstitial atoms in body-centered cubic metals," *Acta Metall.*, **3**[6], 533-537 (1955).
22) S. Taketomi, R. Matsumoto, N. Miyazaki, "Atomistic study of hydrogen distribution and diffusion around a {112}<111> edge dislocation in alpha iron," *Acta Mater.*, **56[**15], 3761-3769 (2008).
23) D. McLean, *Grain boundaries in metals*, Oxford University Press, (1957).
24) R. A. Oriani, "The diffusion and trapping of hydrogen in steel," *Acta Metall.*, **18**[1], 147-157 (1970).
25) J. P. Hirth, "Effects of hydrogen on the properties of iron and steel," *Metall. Trans.*, **A11**[6], 861-890 (1980).
26) H. Sugimoto, Y. Fukai, "Solubility of hydrogen in metals under high hydrogen pressures: thermodynamical calculations," *Acta Metall.*, **40**[9], 2327-2336 (1992).
27) E. H. Du Marchie van Voorthuysen, N. C. Chechenin, D. O. Boerma, "Low-temperature extension of the Lehrer diagram and the iron-nitrogen phase diagram," *Metall. Mater. Trans.*, **A33**[8], 2593-2598 (2002).
28) J. R. Rice, J. S. Wang, "Embrittlement of interfaces by solute segregation," *Mater. Sci. Eng.*, **A107**[C], 23-40 (1989).
29) M. Wen, X. Xu, S. Fukuyama, K. Yokogawa, "Embedded-atom-method functions for the body-centered-cubic iron and hydrogen," *J. Mater. Res.*, **16**[12], 3496-3502 (2001).
30) M. Riku, R. Matsumoto, S. Taketomi, N. Miyazaki, "Atomistic simulation study of cohesive energy of grain boundaries in alpha iron under gaseous hydrogen environment," *J. Soc. Mater. Sci., Japan*, **59**[8], 589-595 (2010), [in Japanese].
31) Y. Fen, C. Wang, "Electronic effects of nitrogen and phosphorous on iron grain boundary cohesion," *Comp. Mater. Sci.*, **20**[1], 48-56 (2001).
32) M. Kim, C. B. Geller, A. J. Freeman, "The effect of interstitial N on grain boundary cohesive strength in Fe," *Scr. Mater.*, **50**[10], 1341-1343 (2004).